Available online at www.sciencedirect.com
ScienceDirect
Ceramics International 35 (2009) 1235–1241
CERAMICS INTERNATIONAL
www.elsevier.com/locate/ceramint

Mechanical behavior of $La_{0.8}Sr_{0.2}Ga_{0.8}Mg_{0.2}O_3$ perovskites

Siddhartha Pathak [a,*], David Steinmetz [a], Jakob Kuebler [b], E. Andrew Payzant [c], Nina Orlovskaya [d]

[a] Department of Materials Science and Engineering, Drexel University, Philadelphia, PA, USA
[b] Empa, Materials Science and Technology, Laboratory for High Performance Ceramics, Duebendorf, Switzerland
[c] Materials Science and Technology Division, Oak Ridge National Laboratory, Oak Ridge, TN, USA
[d] Department of Mechanical, Materials, and Aerospace Engineering, University of Central Florida, Orlando, FL 32816, USA

Received 6 February 2008; received in revised form 19 May 2008; accepted 14 June 2008
Available online 22 July 2008

Abstract

This paper examines the important mechanical properties of commercially purchased $La_{0.8}Sr_{0.2}Ga_{0.8}Mg_{0.2}O_3$ at room temperature and 800 °C. Sr and Mg-doped lanthanum gallates (LSGM) are strong candidates for use as solid electrolytes in lower temperature solid oxide fuel cells operating at or below 800 °C. The material was found to be phase pure with a Young's modulus value of ~175 GPa. The four point bending strength of the LSGM samples remained almost constant from 121 ± 35 MPa at room temperature to 126 ± 20 MPa at 800 °C. The fracture toughness, as measured by the single edge V notch beam (SEVNB) method, was 1.22 ± 0.06 MPa$\sqrt{m}$ at room temperature, 1.04 ± 0.09 MPa$\sqrt{m}$ at 700 °C followed by a small increase 1.31 ± 0.16 MPa$\sqrt{m}$ at 800 °C. We also report, for the first time, the static subcritical (or slow) crack-growth (SCG) behavior of natural cracks in LSGM performed in four point bending tests at room temperature. The exponent of a power-law representation in the SCG tests was found to be $n = 15$, a rather low value showing LSGM to be highly susceptible to room temperature SCG.

Keywords: C. Fracture; C. Mechanical properties; D. Perovskites; E. Fuel cells; Slow crack growth

1. Introduction

Great efforts have been made in recent years by researchers to identify new electrolyte materials in order to reduce the operating temperature of the solid oxide fuel cell (SOFC) from 900–1000 °C (zirconia electrolyte) to 600–800 °C [1]. Decreasing the operating temperature of SOFCs provides a greater selection of materials for the balance of plant or cell stacking which help decrease the fuel cell costs. Sr and Mg-doped lanthanum gallates ($LaGaO_3$), commonly referred to as LSGM, are being considered as an alternative to doped-zirconia electrolytes, especially at intermediate temperatures [2]. These materials, which are based on a perovskite lattice (ABO_3), were found to have high oxide-ion conductivities over a wide range of oxygen partial pressures [3–5]; they demonstrate an oxide-ion conductivity ≥0.126 S/cm at 800 °C, a negligible electronic conduction at temperatures $T < 1000$ °C over a broad range of oxygen partial pressure from pure oxygen ($P_{O_2} = 1$ atm) to moistened hydrogen ($P_{O_2} \sim 10^{-22}$ atm), and a stable performance over long operating times. The highest values of pure oxide-ion conductivity of 0.166 and 0.079 S/cm were found for $La_{0.8}Sr_{0.2}Ga_{0.83}Mg_{0.17}O_{0.2815}$ at 800 and 700 °C, respectively. These properties make it a strong candidate for use as a solid electrolyte in lower temperature solid oxide fuel cells (LT SOFCs) operating at or below 800 °C [6,7].

For practical applications of the SOFC with an LSGM electrolyte, the device must survive consecutive operation for thousands of hours in an elevated temperature range. In addition, it must also be able to withstand thermal stress caused by the resulting temperature gradient and the incompatibility of the thermal expansion between the electrolyte and the bilateral electrodes in the heating or cooling process because the SOFC often experiences a cyclic temperature history at startup and shutdown. Thermal shock resistance is another concern for building a rapid heating ceramic system. The materials should withstand thermal cycling from room temperature to operation temperature ~600–900 °C with a rapid heating and cooling rate

* Corresponding author at: 3141 Chestnut Street, LeBow 344, Philadelphia, PA 19104, USA. Tel.: +1 267 243 9492; fax: +1 215 895 6760.
E-mail address: sp324@drexel.edu (S. Pathak).

0272-8842/$34.00
doi:10.1016/j.ceramint.2008.06.013

~250–500 °C/min. For such reasons, it is absolutely essential to verify the mechanical properties of the LSGM ceramics at both room and elevated temperatures to facilitate practical applications of the multilayered SOFCs containing this electrolyte [3,8–10].

A few recent studies have reported data for the mechanical properties of some gallate compositions as summarized in Table 1. Apart from this, Liu et al. [16] have measured the 3-point bending strength of $La_{0.85}Sr_{0.15}Ga_{0.85}Mg_{0.15}O_{2.85}$ as a function of density where the strength decreases from 183.7 ± 13.7 MPa to 89.9 ± 8.7 MPa when the relative density is reduced from 98.5% to 91.5%. Yasuda et al. [12] have found that the addition of 2 wt.% alumina greatly increases the 3-point bending strength of $La_{0.9}Sr_{0.1}Ga_{0.8}Mg_{0.2}O_{2.85}$ from 120 to 255 MPa at room temperature and from 80 to 190 MPa at 800 °C in air without deleteriously affecting the thermal expansion coefficient and the conductivity of the electrolyte. It is noted that all the studies that used the 'ring-point' or the 3-point bending tests reported higher strength values due to a lower tested surface area or volume as compared to 4-point bend bar testing [17]. Stevenson et al. [15] noted that the SEM inspection of surfaces fractured at various temperatures under four point bending showed that the fracture was predominantly transgranular. Flaw sizes varied from ~10 to 50 μm. Thus the strength of LSGM is comparable to the strength of alkaline earth doped lanthanum chromites and is somewhat lower than the strength of cubic yttria-stabilized zirconia (~250 MPa).

The fracture toughness of $La_{0.9}Sr_{0.1}Ga_{0.8}Mg_{0.2}O_{3-\delta}$, as measured by single edge-notch beam analysis, has been reported as ~2.0–2.2 MPa$\sqrt{m}$ at room temperature, decreasing to ~1.0 MPa$\sqrt{m}$ at 1000 °C [15,18]. The same authors [15] have also used the Vickers indentation method to measure the fracture toughness of the same material as 0.9–1.1 MPa$\sqrt{m}$ at room temperature while noting that the indentation technique generally gives lower values as compared to the macroscopic methods. Another study also used the Vickers indentation technique to measure the fracture toughness of $La_{0.9}Sr_{0.1}Ga_{1-x}Mg_xO_{3-\delta}$ as ~1.63 MPa$\sqrt{m}$ for $x = 0.15$ and ~1.28 MPa$\sqrt{m}$ for $x = 0.2$ [13].

While a lot of work has been done to investigate the mechanical properties of LSGM after preparation, it is also important to analyze the same after a discrete time in the operational environment. Cracks in ceramics are usually initiated at a defect introduced during fabrication or processing [19]. The effect of the environment can lead to the growth of these defects under a constant (or cyclic) load to the point when a critical crack size is reached and unstable crack growth follows. Such a phenomenon is called subcritical or slow crack growth (SCG). Although such a study has been done for a variety of ceramics and other materials, to our knowledge we are the first group to report SCG study on LSGM ceramics.

In this work, we report a combination of mechanical properties for $La_{0.8}Sr_{0.2}Ga_{0.8}Mg_{0.2}O_3$ perovskites at both room and high (700 and 800 °C) temperatures. The properties studied include Young's modulus, strength, fracture toughness and SCG behavior.

2. Experimental procedure

Sintered bars of $La_{0.8}Sr_{0.2}Ga_{0.8}Mg_{0.2}$ Oxide (LSGM) were produced by Praxair Surface Technologies, Specialty Ceramics, USA. The sintered bars were machined to 48.0 mm × 4.0 mm × 2.8 mm size. The grain size in the samples was measured using the intersect technique from the thermally etched surfaces using the Hitachi S-4700 & S-800 Field Emission scanning electron microscopes (SEM).

X-ray powder diffractions (XRD) of the crushed bars were carried out on a Scintag PADV diffractometer (Cu Kα radiation) in 10–80° 2θ range with 0.02° angular step and collection time of 8 s/step. JADE software (Materials Data Inc., Livermore, CA, USA) was used to identify the XRD peaks in the material.

Table 1
Literature values of the bending strengths of lanthanum gallate-based ceramics

Composition	Bending strength (MPa)	Test method	Ref.
$La_{0.9}Sr_{0.1}Ga_{0.8}Mg_{0.2}O_{2.85}$	162 ± 14 (RT) 55 ± 11 (900 °C)	'Ring-point' or ball-on-3-ball test	[11]
$La_{0.9}Sr_{0.1}Ga_{0.8}Mg_{0.2}O_{2.85}$	120 (RT) 80 (800 °C)	3 point bending test	[12]
$La_{0.8}Sr_{0.2}Ga_{0.9}Mg_{0.1}O_{3\pm\delta}$ $La_{0.8}Sr_{0.2}Ga_{0.85}Mg_{0.15}O_{3\pm\delta}$ $La_{0.8}Sr_{0.2}Ga_{0.8}Mg_{0.2}O_{3\pm\delta}$	157 ± 15 (RT) 140 ± 20 (RT) 113 ± 8 (RT)	3 point bending test	[13]
$La_{0.8}Sr_{0.2}Ga_{0.8}Mg_{0.2}O_{3-\delta}$	180 ± 16 (RT) 113 ± 11 (800 °C)	3 point bending test	[14]
Extruded $La_{0.8}Sr_{0.2}Ga_{0.9}Mg_{0.1}O_{2.8}$	287 (RT) 195 (600 °C) 184 (800 °C) 147 (1000 °C)	3 point bending test	[3]
$La_{0.9}Sr_{0.1}Ga_{0.8}Mg_{0.2}O_{3-\delta}$	~150 (RT) 100 ± 10 (600–1000 °C)	4 point bending test	[15]

Bending strengths of lanthanum gallate based ceramics.

The bulk density of all the machined specimens was measured by Archimedes method [20]. The density of the machined specimens was also measured using the Helium Pycnometer, AccuPyc 1330 (Micromerities Instrument Corporation, GA, USA). XRD measurements were used to calculate the theoretical density of the samples. The porosity in the samples was then estimated from the difference between the values of theoretical and bulk density.

Young's modulus (E) for all the samples was measured by impulse excitation method [21] using a Grindo-Sonic Mk5 Industrial (Lemmens, Germany). The Young's modulus at room temperature was also calculated as the slope of the stress deflection curve of the 4-point bending test using a 40/20 mm load geometry at a cross-head displacement speed of 0.4 mm/min (Universal Testing Machine UPM-Zwick 1478, Germany). Deflection of the specimen during loading and unloading was measured with the help of three pushrods. The two outer pushrods were spaced at a distance of 20 mm to correspond with the location of the upper two rollers of the bend fixture. The middle rod was placed midway between the two outer rods. The deflection of the specimen was measured as the deflection of the centre pushrod with respect to the outer rods.

Four-point bending strength was also measured using a 40/20 mm load geometry. The tests were carried out at room temperature with a cross-head displacement speed of 1 mm/min (USM, Zwick Z005, Germany). The high temperature tests were conducted with a cross-head displacement speed of 0.1 mm/min (Universal Testing Machine UPM-Zwick 1478, Germany) after heating at 10 °C/min to a temperature of 800 °C and allowing the sample to equilibrate for 30 min at this temperature prior to testing, in accordance with EN 843-1 [22]. At each temperature, five samples were taken to failure.

Cyclic loading tests were carried out in order to determine if these samples exhibited nonlinear elastic behavior as reported for some other perovskite materials [23] and also to measure the modulus in tension and compression over several cycles. These tests were carried out using strain gauges in the traditional four-point bending test with a 40/20 load geometry on a Zwick 100 testing machine (Universal Testing Machine UPM-Zwick 1478, Germany). The bend bars were fitted with a strain gauge whose coefficient of thermal expansion (CTE = $11 \times 10^{-6}\,K^{-1}$) was very close to that of LSGM (CTE = $10 - 11 \times 10^{-6}\,K^{-1}$). One strain gauge was applied to each 4 mm side of the sample in order to measure both tensile and compressive strain in the sample. The strain gauges were applied directly in the center of the sample and adhered to the sample using rapid adhesive Z 70. The proper loads were calculated with the elastic beam equation. Each successive loading loop was larger than the previous one. The successive stresses were 20, 40, 60, 80, 100, and 120 MPa. A crosshead displacement of 0.3 mm/min was used.

K_{Ic} was measured using the single edge V notch beam (SEVNB) method [24]. The notches were inserted using a specifically constructed notching machine and the final notching was performed using 1 μm diamond paste and a steel razor blade [25,26]. The K_{Ic} values were measured at room temperature, 700 and 800 °C in air. The crosshead displacement speed was 0.3 mm/min for room temperature measurements (USM, Zwick Z005, Germany) and 0.1 mm/min for high temperature measurements (Universal Testing Machine UPM-Zwick 1478, Germany). Three specimens of each composition were tested at each temperature. Fractographic analysis was carried out on selected specimens using the SEM (Tescan Vega Plus 5136 MM SEM, Field Emission Environmental SEM, FEI/Phillips XL30, Hitachi S-4700 & S-800 Field Emission SEMs).

SCG tests under static loads were performed in air according to [27]. The tests were performed in a specifically constructed dead-load equipment. The apparatus was decoupled from the surrounding vibration or shock. The bar-specimens were loaded in four-point flexure using a 40/20 mm load geometry at stresses of 81, 90 and 100 MPa. Five specimens were tested at each stress level. The sample bars were kept under a constant stress at constant temperature and humidity (22 °C and 55% humidity corresponding to a partial pressure of water vapor of ~1.5 kPa) and the time to failure was recorded using an automatic stop watch built on the machine. For these static lifetime tests a time limit of 168 h (7 days) was chosen as specified in [28].

SCG is a time dependant phenomenon where a crack is growing at a constant load such that the applied stresses is less than that needed for instantaneous fracture [19,29]. The crack grows until it eventually attains a critical load-dependent size (a_c) at which the strain energy release rate of the specimen exceeds the fracture resistance of the material for unstable fracture to occur and unstable crack extension follows. This happens at $K_I = K_{Ic}$, where K_I is a stress intensity factor and K_{Ic} is the fracture toughness given by

$$K_{Ic} = \sigma\sqrt{a_c}Y \tag{1}$$

where σ is the stress value and Y is the geometric correction factor dependent on the shape of the crack and the component.

For SCG tests conducted under constant load, the following equation can be derived (for the details of the derivation, see [19,29])

$$t_f = B{\sigma_c}^{n-2}\sigma^{-n} \tag{2}$$

where t_f is the time to failure, B is a material parameter, σ is the applied stress and σ_c is the so called inert strength or the strength without the influence of the slow crack growth. In its logarithmic form Eq. (2) reads as

$$\log t_f = -n\log\sigma + \log\left(B{\sigma_c}^{n-2}\right) \tag{3}$$

From this relation the parameter n can be obtained by linear regression of $\log(t_f)$ versus $\log(\sigma)$. The value of n at room temperature is usually between ten to several hundred. To ensure a high resistance to subcritical crack growth, the exponent n in Eq. (2) should be as high as possible. The lower it is, the more susceptible a material is to subcritical (slow) crack growth at the prevalent environmental conditions.

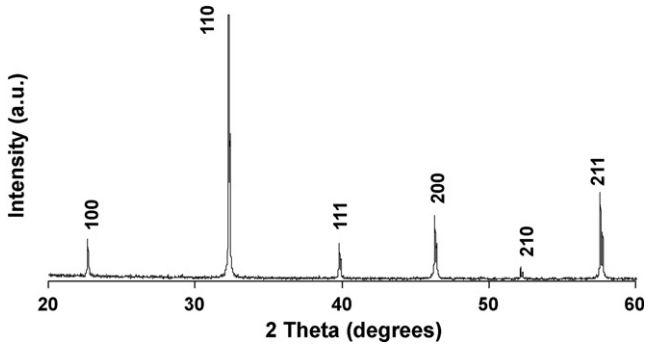

Fig. 1. X-ray diffraction pattern for $La_{0.8}Sr_{0.2}Ga_{0.8}Mg_{0.2}O_3$ perovskites.

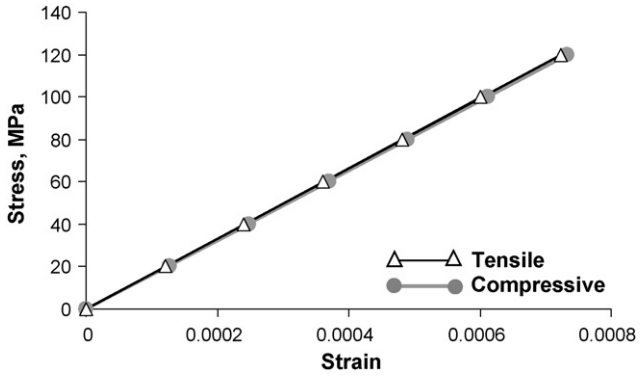

Fig. 2. Compressive and tensile strains in $La_{0.8}Sr_{0.2}Ga_{0.8}Mg_{0.2}O_3$ perovskites during cyclic loading.

3. Results and discussion

3.1. Density, phase composition and Young's modulus

Since LSGM is used as electrolyte for SOFC, it needs to be dense to prevent transport of gases through it. The samples provided by Praxair Surface Technologies, Specialty Ceramics have a suitably low porosity (less than 5%) and that is why they can be used as a good representation of the intermediate temperature SOFC electrolyte materials. These samples have been found to be phase pure by XRD, which shows the presence of only the LSGM cubic phase without any secondary phases (Fig. 1). The average grain size of the samples was found to be 9.0 ± 0.5 μm (Table 2). The behavior of the LSGM samples in 4-point bending was purely elastic during both loading and unloading without any non-linear deformation, as illustrated in Fig. 2. This was also reflected in the identical values of Young's modulus as calculated by the two different test methods; 175 ± 4 GPa as measured by the Natural Frequency method and 176 ± 0.2 GPa as measured by the 4-point bending test (Table 2). These values compare well with the values reported in literature [13] for the same composition (180 ± 4 GPa for $La_{0.8}Sr_{0.2}Ga_{0.8}Mg_{0.2}O_{3-\delta}$).

3.2. Strength and fracture toughness

The strength of LSGM ($La_{0.8}Sr_{0.2}Ga_{0.8}Mg_{0.2}O_3$) remains almost constant from 121 ± 35 MPa at room temperature to 126 ± 20 MPa at 800 °C (Fig. 3) and does not show the decrease in strength with increase in temperature reported in the literature [11,14,15]. The room temperature values in this work are a little lower than what is reported in literature for 4-point bending tests (~150 MPa for $La_{0.9}Sr_{0.1}Ga_{0.8}Mg_{0.2}O_{3-\delta}$ [15]).

Table 2
Density, porosity and Young's modulus of $La_{0.8}Sr_{0.2}Ga_{0.8}Mg_{0.2}O_3$ perovskites as measured by different techniques

Density by Archimedes method	6.24 gm/cc
Density by helium pycnometer	6.28 gm/cc
Theoretical density	6.58 gm/cc
Porosity	5.1%
Young's modulus (natural frequency)	175 ± 4 Gpa
Young's modulus (bending test)	176 ± 0.2 Gpa
Average grain size	9 ± 0.5 μm

However the high temperature strength values at 800 °C in this work are considerably higher than what is reported by Drennan et al. [11] (55 ± 11 MPa at 900 °C for $La_{0.9}Sr_{0.1}Ga_{0.8}Mg_{0.2}O_{2.85}$ using a 'ring-point' or ball-on-3-ball test) and agree well with the values reported by Stevenson et al. [15] (100 ± 10 MPa over the range 600–1000 °C). However all the values for LSGM are somewhat lower than the mechanical strength of fully stabilized zirconia (~300 MPa at room temperature and 120 MPa at 1000 °C) and yttria-tertagonal zirconia ceramics (~1000 MPa at room temperature and 350–400 MPa at 1000 °C) [11]. SEM inspection of surfaces fractured at various temperatures showed that the fracture was predominantly transgranular at both room (Fig. 4a) and high temperatures (Fig. 4b). Flaw sizes varied from ~50 to 70 μm. Because of the transgranular mode of fracture it was not possible to estimate the grain size of the LSGM samples from the fractured surfaces.

For LSGM the K_{Ic} values in this work remains almost constant till 700 °C (1.22 ± 0.06 MPa$\sqrt{m}$ at room temperature, 1.04 ± 0.09 MPa$\sqrt{m}$ at 700 °C) followed by a small increase at 800 °C (1.31 ± 0.16 MPa$\sqrt{m}$), as shown in Fig. 3. In literature, the fracture toughness of LSGM of almost the same density (95–98% dense), as measured by notched beam analysis, has been reported as ~2.0–2.2 MPa$\sqrt{m}$ at room temperature, decreasing to ~1.0 MPa$\sqrt{m}$ at 1000 °C [15,18] These values

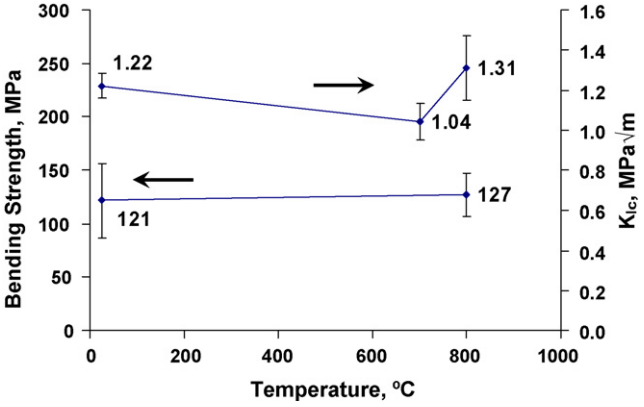

Fig. 3. 4 point bending strength and fracture toughness (K_{Ic}) results for $La_{0.8}Sr_{0.2}Ga_{0.8}Mg_{0.2}O_3$ perovskites. The error bars represent the standard deviation of the values.

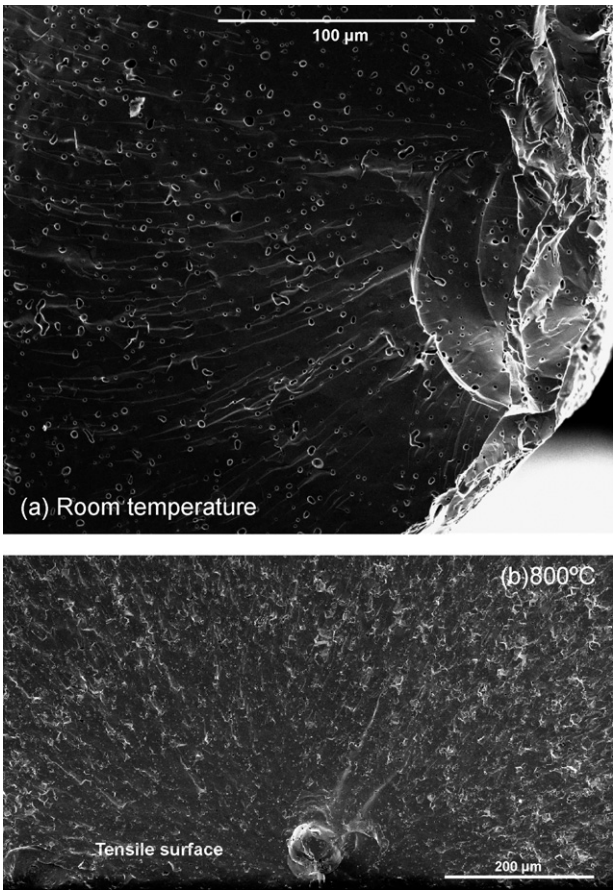

Fig. 4. Fracture origins of $La_{0.8}Sr_{0.2}Ga_{0.8}Mg_{0.2}O_3$ ceramics at (a) room temperature (edge defects) and (b) 800 °C (enclosed granule formed during processing and present near the edge of the specimen). The fracture mode is predominantly transgranular at both the temperatures.

reported in literature are somewhat higher, which is probably due to the different technique (SENB method) being used in which the notch is not as sharp as in the SEVNB method and therefore an overestimation is possible.

3.3. Static subcritical (or slow) crack growth

Subcritical crack growth can occur in brittle materials at stress levels below that required to cause instantaneous failure. This effect is generally caused by the environment. The scatter in the lifetime of a sample depends on the critical flaw size distribution and therefore the scatter in lifetime also correlates to the initial strength scatter [28].

The static subcritical crack growth tests for LSGM were carried out at 22 °C and 55% humidity. Fractography of the LSGM specimens taken from the static lifetime tests was conducted for the specimens with the mean lifetimes at each stress level. It was found that only flaws touching or located near the tensile surfaces of the bend bars initiated the fractures. Fig. 5 shows the surface for a SCG sample tested at 90 MPa (lifetime 0.8 h). Although it is generally difficult to detect the zone of SCG growth in a micrograph, it may be possible to identify the same in this sample. In Fig. 5, the probable initial crack shape (crack shape before static stress was applied), the

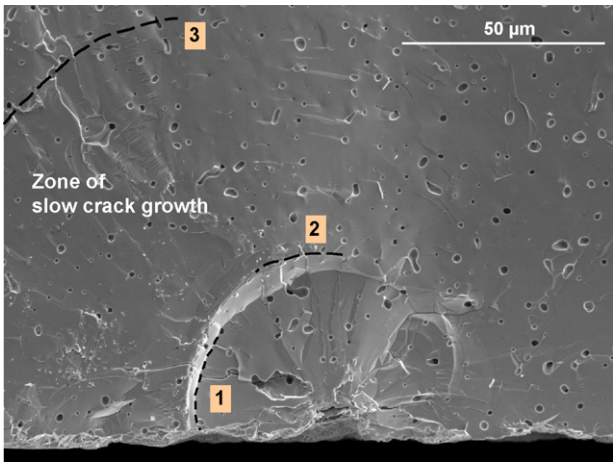

Fig. 5. Fracture surface for SCG tests on $La_{0.8}Sr_{0.2}Ga_{0.8}Mg_{0.2}O_3$ samples (static stress 90 MPa, lifetime 0.8 h, air, 22 °C, 55% humidity). The dotted lines in the micrograph represent: (1) the probable initial preexisting crack, (2) crack front after redirection into the crack plane and (3) the probable final crack size. Assuming this representation to be correct, the area between the lines 1 and 3 would then represent the zone of slow crack growth.

crack front after redirection into crack plane and the probable final crack shape (crack shape after SCG, just before rupture) are indicated by the dotted lines 1, 2 and 3, respectively. To verify these crack shapes, the fracture toughness was estimated using Eq. (1) and assuming $Y \approx 1.29$ [30]. In Fig. 5, for the considered final crack shape at the stress of fracture (90 MPa), the fracture toughness was estimated to be $\sim$1.17 MPa$\sqrt{\text{m}}$. This value corresponds well with the fracture toughness value of 1.22 MPa$\sqrt{\text{m}}$ calculated from SEVNB method given in Fig. 3. Consequently, the area between the dotted lines 1 and 3 in Fig. 5 could correspond to the zone of slow crack growth controlled by the test environment for LSGM.

Assuming that the power law relationship in Eq. (2) is valid, the stresses applied are plotted against the resulting lifetimes in a log(time to failure) − log(stress) diagram in Fig. 6. The value for n of this curve, where $-1/n$ is the slope of the straight line joining the median values for time to failure at each static stress

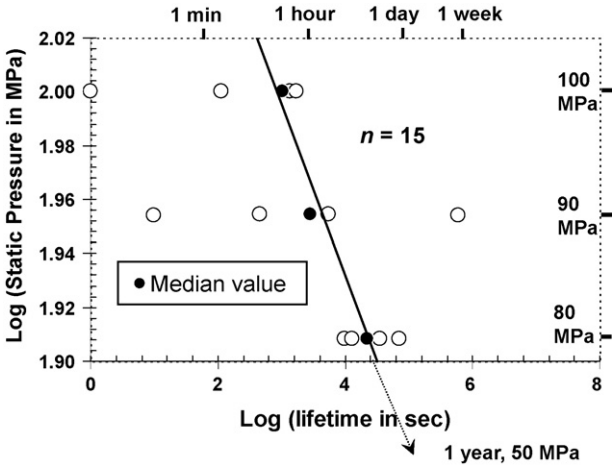

Fig. 6. Log–log diagram of static pressure for static subcritical crack growth vs. lifetime of $La_{0.8}Sr_{0.2}Ga_{0.8}Mg_{0.2}O_3$ perovskite samples at 22 °C and 55% humidity. Samples were tested at 3 static stress levels of 81, 90 and 100 MPa.

level, was found to be 15. Literature values of n for Al_2O_3 ceramics have been reported to be between 50 and 70 [19,31]. Thus the n values for LSGM is quite low indicating that this material is highly susceptible to slow crack growth at room temperature and humid air condition.

While the advantages of this method include a simple test method and analysis technique and the fact that crack growth data are determined for specimens with natural and not artificially induced cracks, these tests do tend to be very time consuming. Also for Eq. (2) a particular type of power law dependency between the crack growth rate and K_I has been assumed [19,29], which can be verified only by separate experiments.

For SOFCs incorporating this LSGM electrolyte, the relationship between time, temperature and lifetime is of importance. Thus, at room temperature, two types of questions may be raised: (i) if a minimum lifetime of 1 year is required, what is the admissible tensile stress? And (ii) if the residual stresses in the SOFC is around 100 MPa (for example), what lifetimes can be expected?

For the first question, using Eqs. (2) and (3), we extrapolate the curve to a lifetime of 1 year (Fig. 6). The admissible tensile stress value is found to be ~50 MPa. Thus at this stress level, 50% of our samples will fail in a period of 1 year. In practice one would expect almost 100% of the sample to survive their designed lifetime, which would mean decreasing the stress value even further. For the 2nd question, following the same logic, the time to failure for 50% of the samples is found to be less than 14 min. It should be emphasized here that these lifetime predictions are valid for parts that are approximately of the same size as the specimens tested. Since the effective surface of LSGM in an actual SOFC is considerably larger, the tolerable stresses, and the attainable lifetimes, are expected to be even lower in practice. The exact dimensions and the stress distributions need to be known if exact calculations are to be made. The inherent assumptions in Eqs. (2) and (3) should also be borne in mind. Tests at higher temperatures (~800 °C) and at the same environment as used in SOFCs also need to be carried out to ascertain the SCG behavior of the samples at the SOFC operating temperatures. Such low stress levels are a cause of concern for a SOFC made of LSGM electrolyte and as such it is unlikely that such materials can be used in electrolyte supported designs for SOFC or in applications where they must play some role in the structural design of a device.

4. Conclusions

Mechanical properties such as Young's modulus, fracture toughness and slow crack growth have been measured for phase pure and highly dense (<5% porosity) $La_{0.8}Sr_{0.2}Ga_{0.8}Mg_{0.2}O_3$ perovskites. The Young's modulus was measured to be ~175 GPa, while strength and fracture toughness both exhibited low values confirming the poor mechanical properties of the material. LSGM was also proved to be highly susceptible to slow crack growth in humid air at room temperature where in order to survive a 1 year period the static stresses in the material should be as low as 50 MPa for a 50% failure probability.

Acknowledgements

The authors would like to thank Mr. R. Baechtold for his help in performing the mechanical tests. This research was supported by the National Science Foundation NSF, DMR (project #0201770). This research was also supported in part by the Assistant Secretary for Energy Efficiency and Renewable Energy, Office of FreedomCAR Vehicle Technologies, as a part of the High Temperature Materials Laboratory User Program, Oak Ridge National Laboratory (ORNL), managed by UT-Battelle, LLC, for the U.S. Department of Energy under contract # DE-AC 05-00OR 22725. S. Pathak also wishes to acknowledge the support from the 2005 SURA-ORNL (the Southeastern Universities Research Association) Summer Cooperative Research Program scholarship and the Thesis grant from Empa, Duebendorf, Switzerland for this work.

References

[1] J.M. Ralph, A.C. Schoeler, M. Krumpelt, Materials for lower temperature solid oxide fuel cells, J. Mater. Sci. 36 (5) (2001) 1161–1172.
[2] K. Huang, J. Wan, J.B. Goodenough, Oxide-ion conducting ceramics for solid oxide fuel cells, J. Mater. Sci. 36 (5) (2001) 1093–1098.
[3] Y. Du, N.M. Sammes, G.A. Tompsett, D. Zhang, J. Swan, M. Bowden, Extruded tubular strontium- and magnesium-doped lanthanum gallate, gadolinium-doped ceria, and yttria-stabilized zirconia electrolytes. Mechanical and thermal properties, J. Electrochem. Soc. 150 (1) (2003) 74–78.
[4] M. Feng, J.B. Goodenough, A superior oxide-ion electrolyte, Eur. J. Solid State Inorg. Chem. 31 (8/9) (1994) 663.
[5] T. Ishihara, H. Matsuda, Y. Takita, Doped $LaGaO_3$ perovskite type oxide as a new oxide ionic conductor, J. Am. Chem. Soc. 116 (9) (1994) 3801–3803.
[6] K. Huang, R.S. Tichy, J.B. Goodeneough, Superior perovskite oxide-ion conductor; strontium and magnesium doped $LaGaO_3$. I. Phase relationships and electrical properties, J. Am. Ceram. Soc. 81 (10) (1998) 2565–2575.
[7] M. Feng, J.B. Goodenough, K. Huang, C. Milliken, Fuel cells with doped lanthanum gallate electrolyte, J. Power Sources 63 (1) (1996) 47–51.
[8] T. Okamuraa, S. Shimizu, M. Mogia, M. Tanimura, K. Furuya, F. Munakata, Elastic properties of Sr- and Mg-doped lanthanum gallate at elevated temperature, J. Power Sources 130 (2004) 38–41.
[9] S.C. Singhal, Advances in solid oxide fuel cell technology, Solid State Ionics 135 (1–4) (2000) 305–313.
[10] J. Wolfenstine, P. Huang, A. Petric, High-temperature mechanical behavior of the solid-state electrolyte: $La_{0.8}Sr_{0.2}Ga_{0.85}Mg_{0.15}O_{2.825}$, J. Electrochem. Soc. 147 (5) (2000) 1668–1670.
[11] J. Drennan, V. Zelizko, D. Hay, F.T. Ciacchi, S. Rajendran, S.P.S. Badwal, Characterisation, conductivity and mechanical properties of the oxygen-ion conductor $La_{0.9}Sr_{0.1}Ga_{0.8}Mg_{0.2}O_{3-x}$, J. Mater. Chem. 7 (1) (1997) 79–83.
[12] I. Yasuda, Y. Matsuzakia, T. Yamakawab, T. Koyama, Electrical conductivity and mechanical properties of alumina-dispersed doped lanthanum gallates, Solid State Ionics 135 (1–4) (2000) 381–388.
[13] N.M. Sammes, F.M. Keppeler, H. Naefe, F. Aldinger, Mechanical properties of solid-state-synthesized strontium- and magnesium-doped lanthanum gallate, J. Am. Ceram. Soc. 81 (12) (1998) 3104–3108.
[14] Y. Du, N.M. Sammes, Fabrication of tubular electrolytes for solid oxide fuel cells using strontium- and magnesium-doped $LaGaO_3$ materials, J. Eur. Ceram. Soc. 21 (6) (2001) 727–735.
[15] J.W. Stevenson, T.R. Armstrong, L.R. Pederson, J. Li, C.A. Lewinsohn, S. Baskaran, Effect of A-site cation nonstoichiometry on the properties of doped lanthanum gallate, Solid State Ionics 113–115 (1998) 571–583.
[16] N. Liu, Y.P. Yuan, P. Majewski, F. Aldinger, Sintering behaviour, mechanical properties and thermal shock resistance of alkaline

earth doped lanthanum gallate, Powder Metall. 49 (1) (2006 March) 34–39.
[17] J. Kübler, R. Primas, B. Gut, Mechanical Strength of Thermally Aged and Cycled Thin Zirconia Sheets, Advances in Science and Technology, Ceramics: Charting the Future, ed. P. Vincenzini, Techna, Florence, Italy, ISBN 88-86538-02-2, pp. 923-928, 1995.
[18] S. Baskaran, C.A. Lewinsohn, Y.S. Chou, M. Qian, J.W. Stevenson, T.R. Armstrong, Mechanical properties of alkaline earth-doped lanthanum gallate, J. Mater. Sci. 34 (16) (1999) 3913–3922.
[19] T. Fett, W. Hartlieb, K. Keller, B. Knecht, D. Münz, W. Rieger, Subcritical crack growth in high-grade alumina, J. Nucl. Mater. 184 (1) (1991) 39–46.
[20] European Standard, EN 623-2, Advanced Technical Ceramics – Monolithic Ceramics – general and Textural properties. Part 2. Determination of density and porosity, September 1993.
[21] preEN 843-2 redraft 3, Methods of test for advanced technical ceramics—Review of ENV 843-2, Determination of elastic moduli at room temperature, February 2004.
[22] EN 843-1, Advanced technical ceramics – Monolithic ceramics – Mechanical properties at room temperature. Part 1. Determination of flexural strength, 1995.
[23] N. Orlovskaya, Y. Gogotsi, M. Reece, B. Cheng, I. Gibson, Ferroelasticity and hysteresis in $LaCoO_3$ based perovskites, Acta Mater. 50 (2002) 715–723.
[24] CEN/TS 14425-5 Advanced technical ceramics—Test methods for determination of fracture toughness of monolitic ceramics. Part 5. Single-edge V-notch beam (SEVNB) method, 2004.
[25] J.A. Salem, M.G. Jenkins, G.D. Quinn, eds., ASTM STP 1409, ASTM, 2002, pp. 93–106, ISBN: 0-8031-2880-0.
[26] J. Kübler, Fracture toughness of ceramics using the SEVNB method: from a preliminary study to a standard test method, Fract. Resist. Test. Monolithic Compos. Brittle Mater. (2002).
[27] European Standard Final Draft, prEN 843-3, Advanced technical ceramics—Monolithic ceramics, mechanical properties at room temperature. Part 3. Determination of subcritical crack growth parameters from constant stressing rate flexural strength tests, November 2004.
[28] J. Kübler, J. Woodtli, K. Berroth, Fractography used with lifetime prediction tests on commercial grades of Alumina and Silicon Carbide, in: J.R. Varner, V.D. Frechette, G.D. Quinn (Eds.), Fractography of Glasses and Ceramics III, The American Ceramic Society, 1996, p. 171.
[29] D. Munz, T. Fett, Ceramics: mechanical properties, failure behaviour, in: Materials Selection 2001, 1st ed., Springer, 2001.
[30] J.C. Newman Jr., I.S. Raju, Empirical stress-intensity factor equation for the surface crack, 15 (1/2) (1981) 185–192.
[31] B.J. Dalgleish, R.D. Rawlings, Comparison of the mechanical behavior of aluminas in air and simulated body environments, J. Biomed. Mater. Res. 15 (4) (1981) 527–542.